Results in Physics 36 (2022) 105410

Contents lists available at ScienceDirect

Results in Physics

journal homepage: www.elsevier.com/locate/rinp

Understanding the role of guest ions in the control of thermal expansion of $FeFe(CN)_6$

Qilong Gao [a,b,*], Yixin Jiao [a], Yi Zheng [a], Andrea Sanson [c,*], Ruggero Milazzo [c], Luca Olivi [d], Qiang Sun [a], Jun Chen [b], Erjun Liang [a]

[a] Key Laboratory of Materials Physics of Ministry of Education, and School of Physics and Microelectronics, Zhengzhou University, Zhengzhou 450052, China
[b] Beijing Advanced Innovation Center for Materials Genome Engineering, School of Mathematics and Physics, Department of Physical Chemistry, University of Science and Technology Beijing, Beijing 100083, China
[c] Department of Physics and Astronomy, University of Padova, Padova I-35131, Italy
[d] Elettra Synchrotron Trieste, I-34149 Basovizza, Italy

ARTICLE INFO

Keywords:
Negative thermal expansion
Vibrational dynamics
Guest species
Tuning of thermal expansion

ABSTRACT

Understanding the role of guest species in framework materials is important to successfully achieve the control of thermal expansion. In this work, the thermal expansion of the Prussian blue analogue $FeFe(CN)_6$ has been effectively tailored from negative, to zero to positive through the insertion of Na^+ ions. To shed light on the role of Na^+ ions on thermal expansion behavior, a joint study was conducted by means of high-resolution synchrotron X-ray diffraction, EXAFS spectroscopy and lattice dynamics calculations. It has been found out that the insertion of Na^+ ions reduces the structural flexibility of the CN linkages and affects the low-energy phonons, thus allowing the tuning of the overall thermal expansion. This work demonstrates the possibility of precisely controlling the thermal expansion of open-framework materials by inserting guest ions and clarifies the physical mechanism underlying this control.

Introduction

Thermal expansion is an important issue in materials applications. However the occurrence of negative thermal expansion (NTE), although quite rare, offers the promising possibility to control the thermal expansion thus enhancing the reliability of materials [1–6]. It is well known that the driving force in many NTE materials depends on the flexibility of the atomic linkages [7–10]. For example, the NTE observed in some metal oxide and fluoride framework materials comes from the transverse vibrations of the central atoms in the M—O—M (M = metal), O—M—O or M—F—M linkages [11–13]. This motion, which has the effect of drawing the two anchoring atoms closer together, increases in magnitude with increasing temperature thus giving rise to the NTE through the so-called "tension" or "guitar-string" effect [14,15]. So it goes without saying that the thermal expansion for this kind of materials can be tuned by changing the structural flexibility. A way to do this is the chemical substitution of the metal ions, which changes the bond strength, reduces the local structure flexibility and hence modifies the thermal expansion behavior [16]. But since the open-framework materials have many voids in their structure, guest species can be inserted thus influencing the dynamics associated with NTE. As example, the thermal expansion coefficient (CTE) of $YFe(CN)_6$ [17] was switched from negative to positive by insertion of K^+ ions and H_2O molecules, or zero thermal expansion (ZTE) was achieved in $ZnPt(CN)_6$ [18] and $TiCo(CN)_6$ [19] by the insertion of H_2O molecules. Kepert and co-workers used adjusted concentrations of CO_2 guest molecules to switch the thermal expansion of two PBAs from negative to positive [20]. Colossal positive thermal expansion was achieved in MCF-34 by inserting polymorphic solvate DMF molecules [21]. Despite these promising results, the continuous tailoring of thermal expansion of open-framework structures by the introduction of guest ions remains very rare.

Cyanide framework materials have gained great attention thanks to their application properties [22], such as gas storage,[23] proton conductivity,[24] energy,[25] environment, [26,27] medicine, [28] and other fundamental physical properties [29], magnetic, electronic and optical properties. Owing to their open structure and framework flexibility, they can display 1D, 2D and 3D NTE behavior [30]. Some metal cyanides, such as HT-CuCN, AgCN, and AuCN [31], exhibit an interesting 1D NTE behavior along the chains direction. $Ni(CN)_2$ exhibits 2D NTE behavior mainly caused by the in-plane rotations of $[NiC_4]$ and

* Corresponding authors.
E-mail addresses: qilonggao@zzu.edu.cn (Q. Gao), andrea.sanson@unipd.it (A. Sanson).

https://doi.org/10.1016/j.rinp.2022.105410
Received 13 December 2021; Received in revised form 16 February 2022; Accepted 8 March 2022
Available online 11 March 2022

[NiN_4] units and rippling of the layers [32]. Other cyanides, such as $Zn(CN)_2$ [33], $CdPt(CN)_6$ [18], $LaFe(CN)_6$ [34] and $Ni_2W(CN)_8$ [35], show a valuable 3D NTE and are promising materials to achieve a ZTE behavior.

Here, we utilize $FeFe(CN)_6$ Prussian blue analogue as case study to tune the thermal expansion from negative to zero to positive through the progressive insertion of guest Na^+ ions. A combined investigation by means of high-resolution synchrotron X-ray diffraction (SXRD), Extended X-ray Absorption Fine Structure (EXAFS) spectroscopy and *ab initio* lattice dynamics calculations was carried out to disclose the role of Na^+ ions on the thermal expansion behavior, from the perspective of the local structure and vibrational dynamics. It turned out that the insertion of Na^+ ions reduces the structural flexibility of the CN linkages affecting the low-energy phonons, thus making possible the tailoring of thermal expansion.

Experimental and computational details

Samples preparation and SXRD characterization

$FeFe(CN)_6{\cdot}xH_2O$ was prepared by solution precipitation method, where 50 mL 0.1 mol/L $Fe(NO_3)_3$ was added to 50 mL 0.1 mol/L $K_3Fe(CN)_6$ aqueous solution. The mixture solution was maintained for 10 h at 60 °C under vigorous stirring. The blue green precipitation was collected by filtration, washed many times by water and ethanol, and then dried at 50 °C for 10 h. Finally, the samples were kept in a black screw cap vial. The anhydrous sample of $FeFe(CN)_6$ was obtained after the dehydration of $FeFe(CN)_6{\cdot}xH_2O$ by heating at 202 °C for 10 h. In the preparation of $Na_{0.8}FeFe(CN)_6{\cdot}xH_2O$, 2 m mol $Na_4Fe(CN)_6{\cdot}10H_2O$ and 2 mL hydrochloric acid (37%) were dissolved in 80 mL deionized water to obtain a homogenous solution. Next steps are the same with $FeFe(CN)_6{\cdot}xH_2O$. The synthesis of $Na_{1.5}FeFe(CN)_6{\cdot}xH_2O$ was the same of $Na_{0.8}FeFe(CN)_6{\cdot}xH_2O$, but it needs to add 2 g NaCl and 1 g K58 in 80 mL deionized water. The content of Na into $FeFe(CN)_6$ was controlled by the amount of Na in solution, which was adjusted by the content of $Na_4Fe(CN)_6$ and NaCl. This preparation method is reported in previous references [36].

The crystal structure of the samples and the lattice thermal expansion were characterized by high-resolution synchrotron x-ray diffraction (SXRD), performed at the 11-BM-B beamline of the Advanced Photon Source (λ = 0.412634 Å). In order to remove the presence of H_2O molecules, the samples have undergone a dehydration process at 475 K, and the SXRD data have been collected under nitrogen atmosphere. The crystal structure was refined through the Rietveld method using the FULLPROF program. [37].

EXAFs

Fe K-edge EXAFS measurements of $FeFe(CN)_6$, $Na_{0.8}FeFe(CN)_6$ and $Na_{1.5}FeFe(CN)_6$ was performed from 475 K to 300 K with a step of 35 K at the XAFS beamline of ELETTRA synchrotron in Trieste (Italy). The sample for EXAFS was prepared by mixing and pelletizing the sample powder with boron nitride powder, with an amount of sample powder chosen to have an absorption edge jump $\Delta\mu x \sim 1$. The Fe K-edge EXAFS spectra were collected in a transmission mode in the energy range of ~6.8–8.4 keV, with an energy step varying from 0.2 eV in the near-edge region to about 4.5 eV at the highest energies, thus to obtain a uniform wave vector step $\Delta k \sim 0.035$ Å^{-1}. The x-ray beam was monochromatized by a Si (1 1 1) double-crystal monochromator. The samples, kept under high-vacuum ($<10^{-5}$ mbar) during the entire experiment, was mounted in a furnace and the temperature was stabilized and monitored through an electric heater controlled by a feedback loop, ensuring a thermal stability within ± 1 K. Two spectra were collected at each temperature point.

The EXAFS data analysis has been performed following the procedure used for $FeFe(CN)_6$ in N. Shi et al [36]. The final results and the corresponding error bars were obtained as average and standard deviation on different spectra, on different k-ranges and best-fitting simulations. We point out that the Fe-N and Fe-C distances, although close, have been distinguished thanks to the inclusion of the second shells and multiple scattering paths in the data analysis procedure. More details on EXAFS analysis can be found in the Supplementary Material.

Computational details

First-principles calculations based on density-functional theory (DFT) were performed using the Vienna *ab initio* simulation package (VASP) [38] with the projector augmented wave (PAW) method. [39] For the treatment of exchange–correlation energy, we employed the generalized gradient approximation (GGA) functional of Perdew–Burke–Ernzerhof (PBE). [40] The kinetic-energy cutoff of the plane-wave basis set was taken to be 520 eV, and the ***k***-space integration was performed with Monkhorst-Pack meshes (9 × 9 × 9). Convergence criteria for the total energy and the ionic relaxation were 10^{-8} eV/atom and 10^{-4} eV/Å, respectively. Vibrational properties were calculated through the PHONOPY code, [41] in which the real space force constants were calculated by employing a 1 × 1 × 1 cell.

Results and discussion

The structure of $FeFe(CN)_6$ is comprised by FeN_6 and FeC_6 octahedra bridged by CN linkages (Fig. 1a), similar to other simple cubic Prussian Blue Analogues (PBAs) such as $ZnPt(CN)_6$[16] and $ScCo(CN)_6$.[30] We could regard the open framework $FeFe(CN)_6$ as A- site deficient perovskite, and the Na^+ ions are located at A- site. The as-prepared samples of $FeFe(CN)_6$, $Na_{0.8}FeFe(CN)_6$ and $Na_{1.5}FeFe(CN)_6$ contain water molecules, which are removed obtaining anhydrous samples after heating at 475 K for 10 h. It should be noted that with the insertion of Na ions, part of Fe atoms reduce the chemical valence from + 3 to + 2 to maintain the chemical equilibrium [42,43]. As shown in Fig. 1a, the XRD patterns at room temperature show that the crystal structures remain cubic even after the Na^+ ions intercalation. Examples of Rietveld refinement are shown in Figs. S4–S6. As the content of Na ions increases, the structure remains cubic until to change to rhombohedral symmetry for $Na_2FeFe(CN)_6$[35]. Accordingly, the samples of $Na0.8FeFe(CN)_6$ and $Na1.5FeFe(CN)_6$ maintain the cubic structure, also on heating. The obtained lattice constant increases from 10.13182(4) Å to 10.33152(3)Å for $FeFe(CN)_6$ and $Na_{1.5}FeFe(CN)_6$, respectively.

As shown in Fig. 1b, $FeFe(CN)_6$ display strong linear NTE (α_l = -4.26 × $10^{-6}K^{-1}$) from 100 to 475 K, which is consistent with the previous report [44]. Interestingly, with the increase of Na content, the thermal expansion can be tuned from NTE to ZTE and then to PTE. ZTE was achieved in $Na_{0.8}FeFe(CN)_6$ (α_l = +0.40 × $10^{-6}K^{-1}$). With the further introduction of Na^+ ions, PTE appears in $Na_{1.5}FeFe(CN)_6$ (α_l = +4.00 × $10^{-6}K^{-1}$). Accordingly, by adjusting the content of Na^+ ions, we can efficiently control the thermal expansion of $FeFe(CN)_6$.

In order to investigate how Na^+ ions act on the thermal expansion behavior of $FeFe(CN)_6$, EXAFS measurements were performed to gain information on the Fe-C and Fe-N atomic pairs. We recall here that EXAFS and X-ray diffraction are complementary techniques. Indeed, while diffraction measures the difference between the average atomic positions, named as the "apparent" bond distance, EXAFS measures the instantaneous atomic distance, named as the "true" bond distance. [45] As shown in Fig. S7, the true and apparent bond distances of both Fe-N and Fe-C show an opposite thermal expansion behavior, the first one expands, the second one contracts. With the Na insertion, the thermal expansion of the apparent bond distance of Fe-N and Fe-C turns to zero and then to positive, while the PTE of the true bond distance is concomitantly weakened.

The atomic mean square relative displacements (MSRDs) for the Fe-N and Fe-C bonds have also been extracted to shed light on the local vibrational dynamics[46]. Fig. 2 shows the temperature dependence of the perpendicular (⊥) and parallel (||) MSRDs of (a-c) Fe-N and (d-f) Fe-C

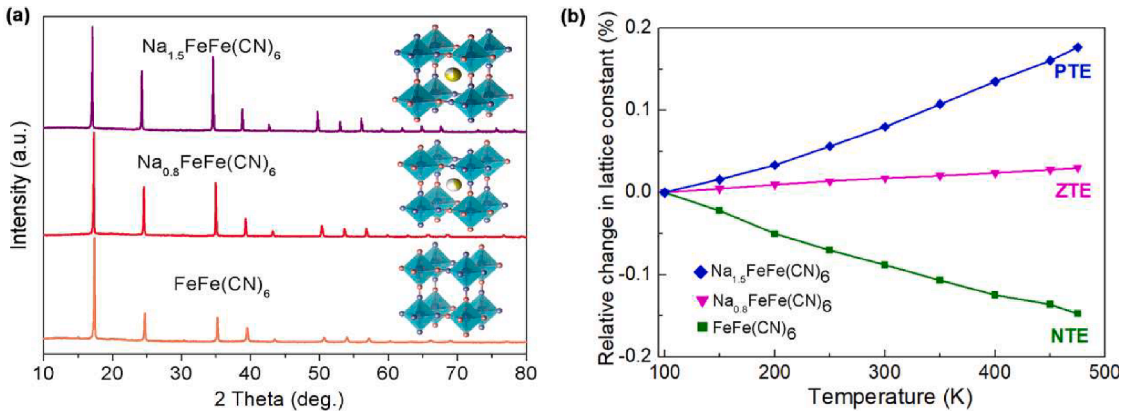

Fig. 1. (a) X-ray diffraction patterns of $FeFe(CN)_6$, $Na_{0.8}FeFe(CN)_6$ and $Na_{1.5}FeFe(CN)_6$ samples at room temperature. Insets show the structure of $FeFe(CN)_6$-based with consisting of corner-shared FeN_6 and FeC_6 regular octahedral, where Na^+ ions are inserted in vacant sites. (b) Relative change of lattice constant with temperature for $FeFe(CN)_6$ (NTE), $Na_{0.8}FeFe(CN)_6$ (near ZTE) and $Na_{1.5}FeFe(CN)_6$ (PTE). Error bars are smaller than the symbols size.

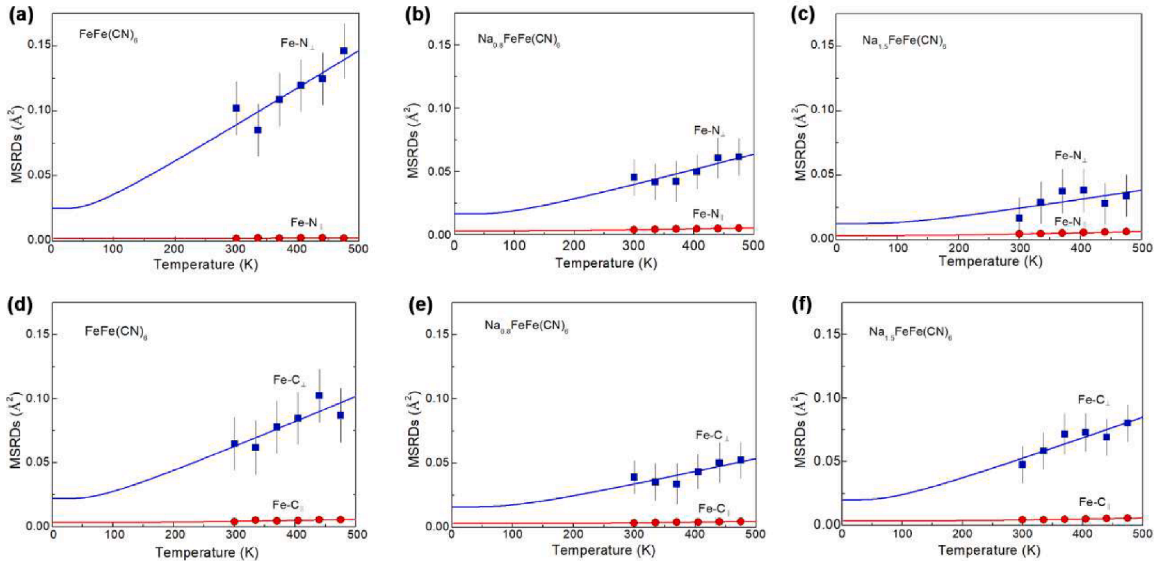

Fig. 2. Temperature dependence of the perpendicular (blue squares) and parallel (red circles) MSRDs of (a-c) Fe-N and (d-f) Fe-C bonds in, from left to right, $FeFe(CN)_6$, $Na_{0.8}FeFe(CN)_6$, and $Na_{1.5}FeFe(CN)_6$. (For interpretation of the references to colour in this figure legend, the reader is referred to the web version of this article.)

bonds in $FeFe(CN)_6$, $Na_{0.8}FeFe(CN)_6$ and $Na_{1.5}FeFe(CN)_6$. In $FeFe(CN)_6$, the perpendicular MSRDs of Fe-N and Fe-C bonds are both much larger than the parallel ones, and the Fe-N perpendicular MSRDs is larger than Fe-C ones. With the insertion of Na^+ ions, the perpendicular MSRD of Fe-N progressively decreases, while that for Fe-C has no marked impact. These results indicate that i) the NTE in $FeFe(CN)_6$-based compounds come from the transverse thermal vibrations of Fe-N atomic pairs and, with less weight, of Fe-C ones; ii) the presence of Na^+ ions has a strong influence on the Fe-N vibrational dynamics.

This is clear from the anisotropy of the relative thermal vibrations (Fig. S8), where it is possible to notice how Fe-N anisotropy decreases strongly with the introduction of Na^+ ions. This is the explanation of how the thermal expansion of $Na_xFeFe(CN)_6$ is switched from negative to zero, to positive. A similar behavior was observed in $Na_xGaFe(CN)_6$ and $K_xYFe(CN)_6$ compounds [15,46] (Fig. S8c).

With the aim of further clarifying the relationship between NTE and vibrational dynamics, *ab initio* calculation based on density functional theory (DFT) were performed in $FeFe(CN)_6$ and $NaFeFe(CN)_6$. Fig. S9 shows the temperature dependence of the lattice volume for $FeFe(CN)_6$ and $NaFeFe(CN)_6$ extracted by DFT calculations which is comparable with the experimental results from SXRD. As shown in Fig. 3a and b, the low-frequency region of the density of vibrational states (DOS) in $FeFe(CN)_6$ and $NaFeFe(CN)_6$ is mainly due to the vibrations of C and N atoms, with N atoms playing a leading role. It should be noted that the contribution of Na atoms is distributed on the low-frequency region below ~200 cm^{-1}. In $FeFe(CN)_6$, a large fraction of low-frequency vibrational modes show a negative Grüneisen parameter (Fig. 3c), in agreement with the presence of a NTE. Once Na is inserted, the negative Grüneisen parameters disappear in a lot of vibrational modes (Fig. 3d), in accordance with the ZTE behavior of $NaFeFe(CN)_6$. As an example, the inset in Fig. 3c shows the eigenvectors of the lowest-frequency vibrational mode with the largest negative Grüneisen parameter (15 cm^{-1}, −17.5) in $FeFe(CN)_6$, where the C and N atoms move perpendicular to the Fe-C-N-Fe linkage. In contrast, in $NaFeFe(CN)_6$, the Grüneisen parameter of the lowest frequency vibrational mode switches to positive (55 cm^{-1}, 4.2), as shown in the inset of Fig. 3d. As a result, the insertion of guest Na^+ ions affect the vibrational dynamics inhibiting the vibrational modes responsible for NTE.

Conclusions

In summary, a continuous tuning of the thermal expansion has been

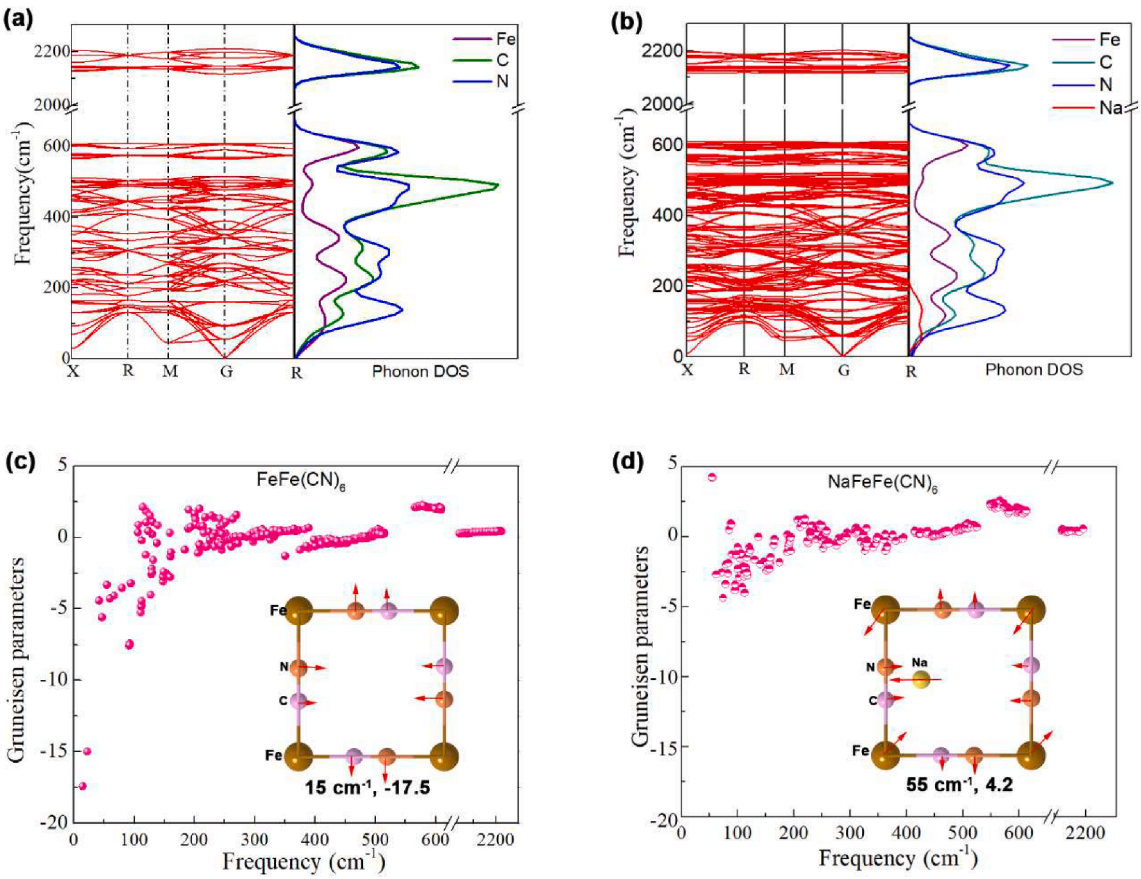

Fig. 3. Phonon dispersion curves and phonon DOS calculated in (a) $FeFe(CN)_6$ and (b) $NaFeFe(CN)_6$. The panels below show the corresponding Grüneisen parameters plotted as a function of the vibrational frequency in (c) $FeFe(CN)_6$ and (d) $NaFeFe(CN)_6$. The insets in panel (c) and (d) show the eigenvectors of the lowest-frequency mode. In $FeFe(CN)_6$ this vibrational mode show the largest negative Grüneisen parameter, while in $NaFeFe(CN)_6$, with the insertion of Na^+ ions, the corresponding Grüneisen parameter switches to positive. Direction and size of arrows reflect the directions and amplitudes of the atomic vibrations.

achieved in $FeFe(CN)_6$ by the insertion of Na^+ ions. The EXAFS results indicated that the NTE of $FeFe(CN)_6$ come from the transverse thermal vibrations of N and C atoms, and the Na^+ ions have the effect of suppressing these vibrations, especially the Fe-N transverse vibrations. DFT calculations show that the low-frequency vibrational modes associated to N and C atoms display negative Grüneisen parameters, and the insertion of Na^+ ions switches these Grüneisen parameters to less negative or positive values, in agreement with the disappearance of the NTE. This work realizes the continuous tuning of thermal expansion of an open-framework material and discloses the role of guest ions in the control of thermal expansion from the perspective of the local vibrational dynamics.

See the Supplementary Material for the sample characterizations and computational methods.

Funding

This work was supported by the National Natural Science Foundation of China (Grant Nos. 22071221, 21905252, 21825102) and Natural Science Foundation of Henan Province (No. 212300410086). All calculations were supported by National Supercomputing Center in Zhengzhou. Elettra Synchrotron is acknowledged for providing beamtime (Experiment n. 20175297) as well as all the staff of XAFS beamline for technical assistance.

Data availability

The data that support the findings of this study are available within this article and its Supplementary Material.

CRediT authorship contribution statement

Qilong Gao: Conceptualization, Investigation, Formal analysis, Writing – original draft, Writing – review & editing. **Yixin Jiao:** Investigation, Formal analysis. **Yi Zheng:** Investigation, Formal analysis. **Andrea Sanson:** Investigation, Formal analysis, Writing – review & editing. **Ruggero Milazzo:** Investigation. **Luca Olivi:** Investigation. **Qiang Sun:** Investigation, Formal analysis, Writing – original draft, Writing – review & editing. **Jun Chen:** Conceptualization, Investigation, Writing – review & editing. **Erjun Liang:** Conceptualization, Investigation, Writing – review & editing.

Declaration of Competing Interest

The authors declare that they have no known competing financial interests or personal relationships that could have appeared to influence the work reported in this paper.

Appendix A. Supplementary data

Supplementary data to this article can be found online at https://doi.org/10.1016/j.rinp.2022.105410.

References

[1] Takenaka K. Sci Technol Adv 2012;13:013001.
[2] Chen J, Hu L, Deng J, Xing X. Chem Soc Rev 2004;44:3522.
[3] Evans JS. J Chem Soc Dalton Tran 1999;19:3317.
[4] Sun Q, Jin K, Huang Y, Guo J, Rungrotmongkol T, Maitarad P, et al. Chinese Chem Lett 2021;32:1515.

[5] Yokoyama T. Microstructures 2021;1:2021003.
[6] Lind C. Materials 2012;5:1125.
[7] Gao Q, Wang J, Sanson A, Sun Q, Liang E, Xing X, et al. J Am Chem Soc 2020;142:6935.
[8] Liang E, Sun Q, Yuan H, Wang J, Zeng G, Gao Q. Front Phys 2021;16:53302.
[9] Goodwin AL, Calleja M, Conterio MJ, Dove MT, Evans JS, Keen DA, et al. Science 2008;319:794.
[10] Mittal R, Gupta MK, Chaplot SL. Prog Mater Sci 2017;92:360.
[11] Wei W, Gao Q, Guo J, Chao M, He L, Chen J, et al. Appl Phys Lett 2020;116:181902.
[12] L. Rimmer, M. Dove, A. Goodwin and D. Palmer, Phys. Chem. Chem. Phys. 2014, **16**, 21144(2014).
[13] Greve BK, Martin KL, Lee PL, Chupas PJ, Chapman KW, Wilkinson AP. J Am Chem Soc 2010;132:15496.
[14] Sanson A. Chem Mater 2014;26:3716.
[15] Gao Q, Sun Y, Shi N, Milazzo R, Pollastri S, Olivi L, et al. Scripta Mater 2020;187:119.
[16] Shi N, Song Y, Xing X, Chen J. Coordin Chem Rev 2021;449:214204.
[17] Gao Q, Chen J, Sun Q, Chang D, Huang Q, Wu H, et al. Angew Chem Int Edit 2017;56:9023.
[18] Goodwin AL, Chapman KW, Kepert CJ. J Am Chem Soc 2005;127:17980.
[19] Gao Q, Shi X, Venier A, Carnera A, Huang Q, Wu H, et al. Inorg Chem 2020;59:14852.
[20] Auckett JE, Barkhordarian AA, Ogilvie SH, Duyker SG, Chevreau H, Peterson VK, et al. Nat Commun 2018;9:4873.
[21] Zhou HL, Lin RB, He C-T, Zhang YB, Feng N, Wang Q, et al. Nat Commun 2013;4:2534.
[22] Gao Q, Liang E, Xing X, Chen J. J Chin Univers 2020;41:388.
[23] Kaye SS, Long JR. J Am Chem Soc 2005;127:6506.
[24] Ohkoshi SI, Nakagawa K, Tomono K, Imoto K, Tsunobuchi Y, Tokoro H. J Am Chem Soc 2010;132:6620.
[25] Ma F, Li Q, Wang T, Zhang H, Wu G. Sci Bull 2017;62:358.
[26] Cao LM, Lu D, Zhong DC, Lu TB. Coord Chem Rev 2020;407:213156.
[27] Q. Gao, J. Chen, Q. Li, J. Zhang, Z. Zhai, S. Zhang, Ranbo. Y, and X. Xing, Inorg. Chem. Front. **5**, 438(2018).
[28] Liu B, Wang W, Fan J, Long Y, Xiao F, Daniyal M, et al. Biomaterials 2019;217:119301.
[29] Tokoro H, Ohkoshi SI. Dalton Trans 2011;40:6825.
[30] Wang J, Gao Q, Gao Y, Luo Y, Guo J, Sun Q, et al. Appl Phys Lett 2021;118:222105.
[31] Hibble SJ, Wood GB, Bilbé EJ, Pohl AH, Tucker MG, Hannon AC, et al. Z Krist-Cryst Mater 2010;11:457.
[32] Hibble SJ, Chippindale AM, Pohl AH, Hannon AC. Angew Chem 2007;119:7246.
[33] Hibble SJ, Chippindale AM, Marelli E, Kroeker S, Michaelis VK, Greer BJ, et al. J Am Chem Soc 2013;44:16478.
[34] Gao Q, Sun Q, Venier A, Sanson A, Huang Q, Jia Y, et al. Sci China Mater 2021.
[35] Wang C, Chang D, Gao Q, Liu C, Wang Q, Huang X, et al. Phys Chem Chem Phys 2020;22:18655.
[36] Li W, Chou S, Wang J, Kang Y, Wang J, Liu Y, et al. Chem Mater 2015;27:1997.
[37] Rodríguez-Carvajal J. Phys B 1993;192:55.
[38] Kresse G, Hafner JJ. Phys Rev B 1996;6:15.
[39] Kresse G, Joubert D. Phys Rev B 1999;59:1758.
[40] Perdew JP, Burke K, Ernzerhof M. Phys Rev Lett 1996;77:3865.
[41] Togo A, Oba F, Tanaka I. Phys Rev B 2008;78:134106.
[42] Y. Lu, L. Wang, J. Cheng J. B. Goodenough, Chem. Commun., **48**, 6544(2012).
[43] Wu X, Jian Z, Li Z, Ji X. Electrochem Commun 2017;77:54.
[44] Shi N, Gao Q, Sanson A, Li Q, Fan L, Ren Y, et al. Dalton Trans 2019;48:3658.
[45] Sanson A. Microstructures 2021;1:2021004.
[46] Gao Q, Shi N, Sanson A, Sun Y, Milazzo R, Olivi L, et al. Inorg Chem 2018;57:14027.